Journal of the Ceramic Society of Japan 118 [8] 706-710 2010 Paper

Cation distribution and piezoelectric properties of aluminum substituted $La_3Ta_{0.5}Ga_{5.5}O_{14}$ single crystals

Hiroaki TAKEDA,† Jun-ichi YAMAURA,* Takuya HOSHINA and Takaaki TSURUMI

Graduate School of Science and Technology, Tokyo Institute of Technology, 2–12–1 Ookayama, Meguro, Tokyo 152–8552
***Institute for Solid State Physics, The University of Tokyo, 5–1–5 Kashiwanoha, Kashiwa, Chiba 277–8581**

We report the structure and electric properties of $La_3Ta_{0.5}Ga_{5.5-x}Al_xO_{14}$ (LTGAx, $x = 0.0$ (LTG), 0.3 and 0.5) single crystals, with a $Ca_3Ga_2Ge_4O_{14}$-type structure, suitable for high temperature piezoelectric application. A single-crystal X-ray structure analysis reveals that Al atoms are distributed in all cation sites except for the decahedral site occupied by La, which favors instead the octahedral site. The piezoelectric moduli d_{11} kept a constant, whereas $|d_{14}|$ increased 14% with the increasing Al content, x, up to 0.5. The LTGA0.5 crystals showed a low temperature dependence (2% deviation from room temperature to 400°C) of d_{11} and a higher electric resistivity ρ than those of the LTG crystals. The Al substitution is effective for improving the electrical properties of the LTG.

Key-words : Oxides, Crystal growth, Crystal structure, Cation distribution, Piezoelectricity, High temperature

[Received March 17, 2010; Accepted May 20, 2010]

1. Introduction

High temperature piezoelectric materials are in high demand for gas sensors, combustion pressure sensors and gas injectors directly placed in the cylinder of engines. The candidates for the sensor material are AlN thick films,[1] $GaPO_4$ crystals,[2] $La_3Ga_5SiO_{14}$ (langasite, LGS)-type crystals,[3] and rare-eath calcium oxoborate $ReCa_4O(BO_3)_3$ crystals.[4)–5] The AlN has high chemical reactivity at high temperatures. Bulk growth of $GaPO_4$ crystals is very difficult, as the $GaPO_4$ crystal transforms into the high-cristobalite phase at 930°C, above which the piezoelectricity of the crystal is drastically abated.[2] The $ReCa_4O(BO_3)_3$ crystal has a very low crystal symmetry monoclinic m, and the determination of piezoelectric modulus have not yet been clarified. Therefore, among them, we paid attention to the LGS-type single crystals because the crystal shows no phase transitions up to its melting temperature, has relatively high crystal symmetry and can be easily grown to a large size using the Czochralski (Cz) technique.[6)–8]

For practical use, the LGS-type crystals need both a low temperature dependence of the piezoelectric properties and a high electric resisitvity ρ at high temperatures. Taishi et al.[9] improved the resistivity of the LGS crystals. The crystals were grown in inert gasses (N_2 or Ar), and the ρ value was $10–10^2$ times higher than that of the LGS crystals grown in the oxygen-containing atmosphere. We have found another way to increase the electric resistivity of the LGS crystals. By substituting Al^{3+} ions for some of the Ga^{3+} ions, we obtained the LGS crystals with a higher electric resistivity.[10] This substitution should be applied to other LGS-type crystals. We have grown and characterized the Al-substituted LTG, $La_3Ta_{0.5}Ga_{5.5-x}Al_xO_{14}$ (LTGAx) single crystals.[10)–11] The crystals showed an improvement in the resistivity similar to that of LGS. Similar observations were reported by Jung et al.[12] and Zhang et al.[13] Thus, although the substitution effect of Al^{3+} for Ga^{3+} in LTG on the electric properties was reported, the effect of Al substitution on the crystal structure and the piezoelectric properties of the LTGAx crystals has not been recognized.

In this paper, we will report the results of an investigation about the structural and piezoelectric properties of LTGAx single crystals. We also describe the detailed electric properties of these crystals at high temperatures.

2. Experimental

The single crystals, with a 18–22 mm diameter and 80–120 mm length, were grown by a conventional Czochralski technique. The melts with three compositions [$x = 0.0$ (i.e., LTG), 0.3, and 0.5] were used as the starting materials because of the Al solubility limit ($x \leq 0.5$) in LTG.[14] The Al content in the crystals (parameter x) was determined by a quantitative X-ray fluorescence (XRF) analysis. The glass-bead technique was used. For measurement sample preparation, top and bottom of the cylinder part of grown crystals were pulverized and the powders were fused with lithium tetraborate. Prior to this preparation, both parts were confirmed to be composed of a LTG-type structure phase by powder X-ray diffraction and scanning electron microscope. For providing calibration curves, standard samples were also prepared with mixture of pure oxides and lithium tetraborate. The analysis was performed through a wavelength dispersive XRF spectrometer using a PANalytical Magi'X Pro.

Structural analyses were performed at room temperature, 23°C, using crystals of an almost spherical shape with 0.116–0.142 mm diameter in a three-circle diffractometer equipped with a CCD area detector (Bruker SMART APEX). Oscillation photographs were taken using a curved imaging plate (MacScience DIP 320 V) and a helium closed-cycle refrigerator. Monochromatic Mo–Kα radiation was used as the X-ray source. Data integration and global-cell refinements were performed with SAINT using data in the range $2\theta = 4–107°$, and absorption correction was applied using SADABS.[15] Symmetry equivalent reflections were averaged to produce unique reflections ($R_{int} = 0.023–0:025$).

† Corresponding author: H. Takeda; E-mail: htakeda@ceram.titech.ac.jp

Structural parameters were refined by the full-matrix, least-squares method using the SHELXL-93.[16] The final residual factor $R[F]$ ($R_w[F^2]$) values were 0.028 (0.060), 0.025 (0.056) and 0.028 (0.067) for $I > 3.0\sigma(I)$ at LTGAx with $x = 0.0$, 0.3 and 0.5, respectively.

In the LTGAx crystals, the independent material constants consisted of two dielectric, two piezoelectric and six elastic compliance constants (ε_{ij}, d_{ij} and s_{ij}, respectively). The material constants were determined using an impedance/gain phase analyzer (HP 4194A: Agilent) as reported in Refs. 17)–19). The electromechanical coupling factor k_{ij} and the piezoelectric modulus were evaluated by measuring the mechanical series resonance frequency f_s and parallel resonance frequency f_p of the equivalent resonators. The equivalent resonators were fabricated in the form of plates according to the length-extensional vibration mode. The dielectric constants ε_{ij} were determined by measuring the capacitances of the resonators by taking the parasitic capacitance into account. The changes in d_{11} and the electric resistivity ρ in the temperature range from room temperature to 700°C were investigated.

3. Results and discussion

We obtained LTGAx single crystals pulled in the ⟨001⟩ direction through the Cz technique. Since no growth instability, such as the spiral symptom, appeared during the growth, the uniform diameter of the grown crystals was easily controlled. **Figure 1** shows the typical LTGA0.3 grown crystals. The crystals showed a smooth surface and were transparent with an orange color. We did not observe any differences in color between the pure LTG and the Al-substituted crystals. Morever, no cracks nor inclusions were found inside the grown crystals. All peaks in the X-ray diffraction patterns of the boules were identified to be those of the LGS-type structure. By XRF analysis, the determined Al-content x of top and bottom of the cylinder part of the LTGAx crystals were as follows: $x = 0.31$ (top) and 0.30 (tail) for LTGA0.3, and $x = 0.54$ (top) and 0.51 (tail) for LTGA0.5. Although segregation phenomena occurred during crystal growth due to LTGAx solid solution crystals, the LTGAx crystals showed small variation in the Al_2O_3 concentration within the investigated composition of this study. These results suggested that the starting melt composition of LTGAx is similar to the composition of the grown crystals. The similar observation was obtained in Al-substituted LGS crystals.[20] In the Ref. 20), the effective segregation coefficient, k_{eff}, of the Al-substituted LGS crystals between 1.03 and 1.07. Therefore, the values for x in this paper are considered to be the same as those of the starting materials.

The LTGAx crystals have the $Ca_3Ga_2Ge_4O_{14}$-type structure (space group: $P321$, $Z = 1$).[21] There are four kinds of cation sites in the structure with the chemical formula $\{E\}_3[A](F)_3\langle D\rangle_2O_{14}$, which is a modified notation using the Wyckoff letter. The crystal structure is schematically shown in **Fig. 2**. The notations {E} and [A] represent a decahedral (twisted Thomson cube) site coordinated by eight oxygens and an octahedral site coordinated by six oxygens, respectively. Moreover, (F) and ⟨D⟩ represent tetrahedral sites coordinated by four oxygens, the size of the ⟨D⟩ site being smaller than that of the (F) site. In the LTG crystal, La^{3+} occupies the {E} sites, Ta^{5+} occupies half of the [A] sites, and Ga^{3+} occupies another half of the [A], (F) and ⟨D⟩ sites.[22] In this paper, the notations {E}, [A], (F) and ⟨D⟩ are defined as La, Ga1, Ga2, and Ga3, respectively. **Table 1** lists the structure refinement results, consisting of the lattice constants and the site occupancies along with other relevant structural information. Both lattice constants, a and c, decrease with increasing Al content in the

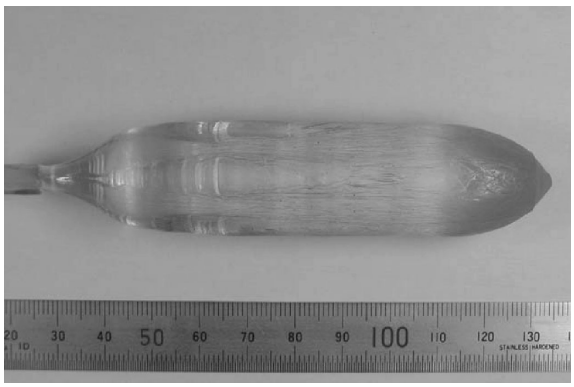

Fig. 1. As grown $La_3Ta_{0.5}Ga_{5-x}Al_xO_{14}$ ($x = 0.3$) single crystal.

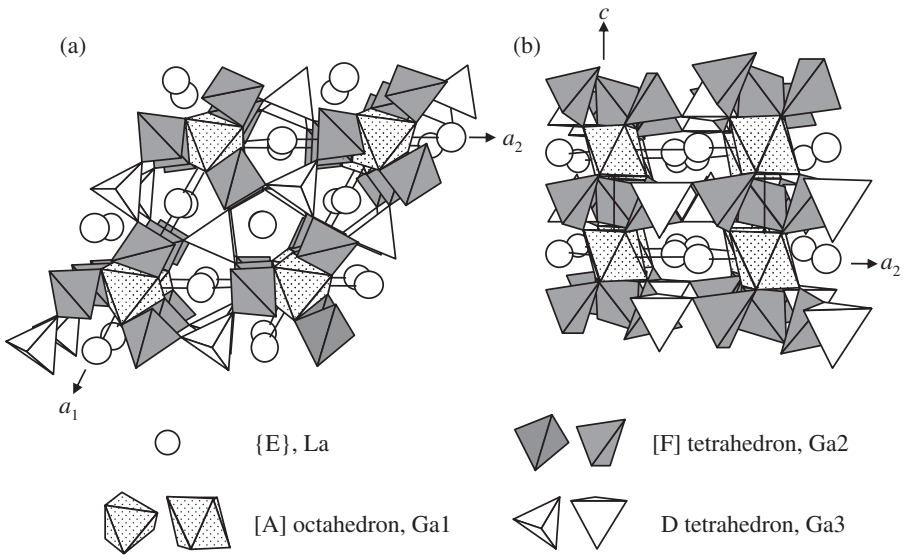

Fig. 2. Schematic illustrations of the $La_3Ta_{0.5}Ga_{5-x}Al_xO_{14}$ crystal structure along (a) [001] and (b) [120] directions (perspective view).

Table 1. Lattice constants, site occupancy, mean oxo-bond distances, and structural distortion of $La_3Ta_{0.5}Ga_{5.5-x}Al_xO_{14}$ crystals

Al-content (x)		0.0	0.3	0.5
Unit cell (±0.0001 Å)				
a		8.2381	8.2295	8.2272
c		5.1287	5.1207	5.1156
V [Å^3]		301.43	300.34	299.87
Calcluated Mass density [g/cm^{-3}]				
D_x		6.140	6.092	6.054
Site occupancies (±0.003)				
Ga1 site[a]	Al		0.082	0.094
	Ga	0.5	0.418	0.406
	Ta	0.5[a]	0.5[a]	0.5[a]
	Al/(Ga + Al)	0	0.164	0.188
Ga2 site	Al	—	0.023	0.049
	Ga	1	0.977	0.951
Ga3 site	Al:	—	0.074	0.130
	Ga	1	0.926	0.870
Mean oxo-bond distances, D_i [Å]				
$(La\text{-}O)_{ave}$	D_8	2.599	2.600	2.599
$(Ga1\text{-}O)_{ave}$	D_6	1.999	1.992	1.991
$(Ga2\text{-}O)_{ave}$	D_4	1.855	1.851	1.849
$(Ga3\text{-}O)_{ave}$	$D_{4'}$	1.834	1.826	1.822
Distortion, Δ (magnified by 10^4)				
La site		47	48	48
Ga1 site[b]		0	0	0
Ga2 site		1.4	0.7	0.7
Ga3 site		0.7	0.9	1.0

[a]On the basis of the result for the LTG sample in Ref. 21), occupancy of the Ta atom in the Ga1 site was fixed of 0.5 during the refinement process.

[b]The structural distortion around the Ga1 site was not determined because all the cation–oxygen interatomic distances were the same. The coordinating oxygens are placed at equivalent position (6g).

crystals. This result is supported by the difference in the cation size ($r_{Al} < r_{Ga}$).[23] Based on the structure refinement result of $La_3Ga_{5-x}Al_xSiO_{14}$ (LGASx),[24] the distributions of Al and Ga in the LTGAx crystals were analyzed by common site-multiplicity refinement. The structural parameters determined suggest that Al atoms occupy all cation sites except for the La site. Finally, for both LTGA0.3 and LTGA0.5 crystals, the distribution model in which the Al atom partially occupies the whole of Ga sites produced minimum R values. That is, the Al and Ga atoms coexist in the octahedral and two tetrahedral sites. The results agreed with those obtained in LGASx. The Al occupancy ratio Al/(Ga + Al) in the Ga1 site (0.164 and 0.188 for LTGAS0.3 and LTGA0.5, respectively) was the highest of those in the other Ga sites, as seen in Table 1. This Al favoring of the octahedral site is also observed in the garnet-type structure, which has similar coordination polyhedrons.[25)–26)] Furthermore, the tetrahedral Ga2 site is obviously lower than the tetrahedral Ga3 one, with respect to site preference. This observation is also found in LGASx crystals.[24]

The mean cation–oxygen distances D_i ($i = 4$, $4'$, 6, and 8) are defined in Table 1. The D_8 value remains constant at about 2.600 Å, though the other D_4, $D_{4'}$, and D_6 values clearly decrease with increasing Al content, as seen in Table 1. The magnitude of the distance changes ($\Delta D_6/\Delta x$:$\Delta D_4/\Delta x$:$\Delta D_{4'}/\Delta x \approx 1.3$:1:2.0) is consistent with that of the Al occupancy ratio ~1.9:1:2.6 in the corresponding sites, derived from site-multiplicity refinement results. This observation also agreed with that obtained in LGASx.[24] We also calculated the structure distortion Δ[23] of each polyhedron unit's coordination, which is defined by

Table 2. Mass density, Electromechanical coupling factors and materials constants of $La_3Ta_{0.5}Ga_{5.5-x}Al_xO_{14}$ (measured at room temperature 23°C)

Al-content (x)		0.0	0.3	0.5
Mass density [g/cm^{-3}]	D_m	6.134(4)	6.064 (4)	5.998(6)
Electromechanical	k'_{12}[a]	0.165	0.166	0.166
coupling factors	k'_{23}[b]	0.061	0.067	0.069
Elastic compliance	s^E_{11}	9.06(2)	9.08(3)	9.09(1)
constants [10^{-12} m^2/N]	s^E_{12}	−4.64	−4.67	−4.68
	s^E_{13}	−1.95	−1.97	−2.02
	s^E_{14}	−3.54	−3.58	−3.70
	s^E_{33}	5.18	5.19	5.27
	s^E_{44}	21.9	21.8	21.8
	s^E_{66}	27.4	27.5	27.6
Piezoelectric constants	d_{11}	6.62(3)	6.62(5)	6.63(2)
[pC/N]	d_{14}	−3.68	−4.03	−4.19
Relative dielectric	$\varepsilon^T_{11}/\varepsilon_0$	20.0(3)	19.9(2)	19.8(2)
constants [—]	$\varepsilon^T_{33}/\varepsilon_0$	79.9	72.0	67.9

[a]vibration mode: Length-extensional (transverse effect) crystal substrate: (XYt)0°

[b]vibration mode: Length-extensional (transverse effect) crystal substrate: (XZt)45°

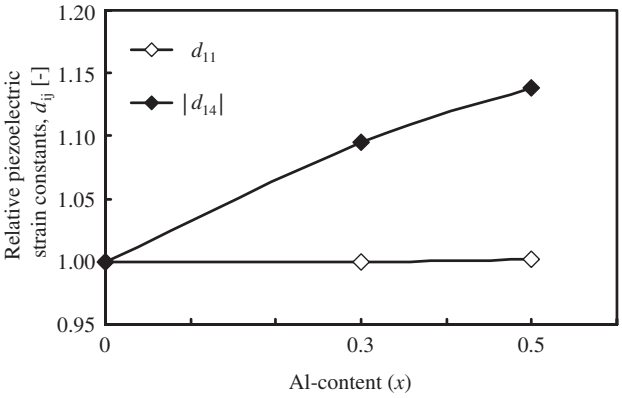

Fig. 3. Variation of piezoelectric strain d_{ij} constants as a function of Al-content for $La_3Ta_{0.5}Ga_{5-x}Al_xO_{14}$ crystals.

$\Delta = (1/N)\sum((R_i - \bar{R}/\bar{R}))^2$, where N is the coordination number (8 for the La decahedron, 6 for the Ga1 octahedron, and 4 for the Ga2 and Ga3 tetrahedrons), R_i is the individual bond length, and $\bar{R}$ is the average bond length. The calculation results are shown in Table 1. As pointed out in Ref. 24), the La decahedron maintains a constant Δ, but the distortion of the Ga2 and Ga3 tetrahedra is sensitive to the Al content. We conclude that the Al substitution was found to affect only the occupying sites (Ga1, Ga2, and Ga3 sites).

The evaluated mass density, electromechanical coupling factors, and material constants of the LTGAx single crystals are shown in **Table 2**. The mass density of LTGAx crystals decreases with increasing Al-content. This proved that Al is incorporated into the grown crystals. The material constants of LTG (LTGA0.0) crystals are consistent with those reported by Bohm et al.[27] and Onozato et al.[28] Electromechanical coupling factors k'_{12} and k'_{23} were measured to determine d'_{12} ($= -d_{11}$) and d'_{23} ($= 0.5d_{14}$), respectively. The k'_{12} value is almost constant but the k'_{14} one increases with increasing Al content. **Figure 3** shows the changes in piezoelectric strain d_{ij} constants as a function of x in LTGAx. With an increase in the Al content, the absolute piezoelectric strain modulus d_{11} remains constant, while d_{14} increases by 14%. The tendency was understood that an

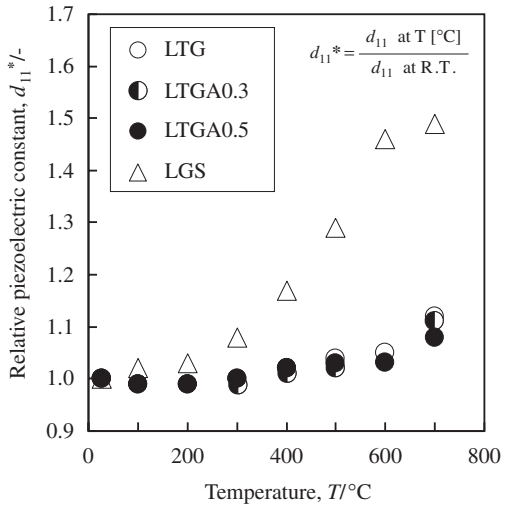

Fig. 4. Relative piezoelectric constant d_{11}* as a function of temperature for $La_3Ta_{0.5}Ga_{5-x}Al_xO_{14}$ crystals.

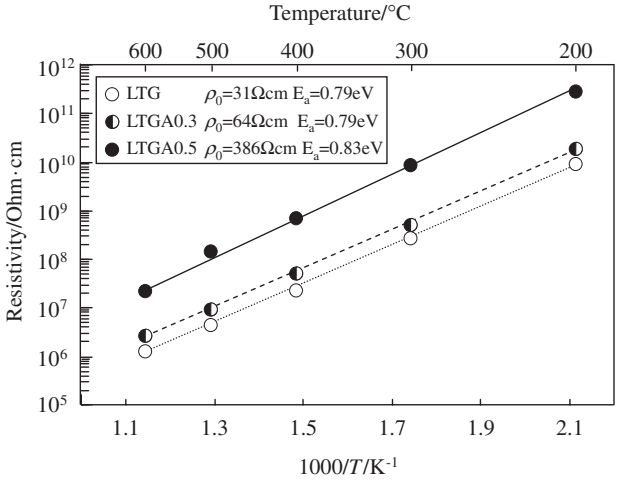

Fig. 5. Resistivity as a function of temperature for $La_3Ta_{0.5}Ga_{5-x}Al_xO_{14}$ crystals.

increment of d_{11} of the $Ca_3Ga_2Ge_4O_{14}$-type crystals occurs when the D_8 is extended against other cation–oxide distances.[24),29)] Actually, in the LGASx crystals, d_{11} increased ~1.3%, and D_8 extended relatively due to the reduction of D_4, D_4, and D_6.[24)] The observation on cation–oxide distances is also seen in the LTGAx crystal in this study. However, the Al-contetnt in the LTGAx crystal is lower than that in the the LGASx crystals. So, the effect of Al substitution on d_{11} constants in the LTGAx crystal is not clear. We found that Al substitution affected the d_{14} constant. The d_{14} constant was calculated using k'_{23}, s^E_{33} and ε^T_{11} based on the following equation,

$$d'_{23}\ (=0.5d_{14}) = k'_{23}\sqrt{s^E_{33}\varepsilon^T_{11}}. \quad (1)$$

With increasing Al content, ε^T_{11} decreased 2.0% whereas s^E_{33} increased 1.7% (see Table 2). However, k'_{23} increased 13% with Al content. Moreover, considering the equation $d_{14} = k_{14}\sqrt{s^E_{44}\varepsilon^T_{11}}$, s^E_{44} almost maintains same values as shown in Table 2. Hence, it is clear that the increment of d_{14} in LTGAx is attributed to the increment of coupling factor k.

Figure 4 shows the temperature dependence of the piezoelectric constant d_{11} of LTGAx and LGS crystals. In this figure, the relative piezoelectric constant d_{11}* represents the ratio of the d_{11} value at the measurement temperature and at room temperature (25°C). The d_{11} increased with temperature for all the crystals. Small differences in thermal behavior were observed between the pure LTG (LTGA0.0) and the Al-substituted crystals. We found that the Al substitution hardly affected the thermal behavior of the piezoelectric properties of the LGS-type crystals. However, since the LTGA0.5 crystals show the smallest change (1.5%) of all the crystals investigated in this study, this crystal is suitable for high temperature use.

Figure 5 shows temperature dependences of electric resistivity ρ of as-grown LTGAx crystals. In this figure, the plots of $\ln\rho$ versus $1/T$ show linear behavior. In all crystals, ρ decreases with increasing temperature. The LTGA0.5 crystal has high ρ values of one order of magnitude, compared with pure LTG crystals at high temperatures. This value is the same level as that reported in the $La_3Nb_{0.5}Ga_{5.3}Al_{0.2}O_{14}$ (Al-substituted $La_3Nb_{0.5}Ga_{5.5}O_{14}$, LNG) crystal.[13)] The ρ value of LTGA0.2 was also reported and was comparable to that of the LTGA0.3 crystal in this study. The ρ value is almost satisfied for the required values at 400°C. Therefore, we found Al substitution is effective in improving the electric resistivity of the LGS-type crystals. The temperature dependences of the resistivity shown in Fig. 5 can be expressed by Arrhenius law:

$$\rho = \rho_0 \exp(E_a/k_BT) \quad (2)$$

where ρ_0 is the resistivity at an infinite temperature, E_a is the activation energy, k_B is the Boltzmann's constant and T is the absolute temperature. The ρ_0 and E_a are also shown in Fig. 5. The activation energy E_a was determined to be 0.79, 0.79 and 0.83 eV for LTG(LTGA0.0), LTGA0.3 and LTGA0.5 crystals, respectively. These values are similar to the data for LGS, Al-substituted LGS, LNG and LTG reported.[10),13),30)] Based on these results, the same conduction mechanism lies in all crystals. The resisitivity of LGS depends on operating partial oxygen pressure during crystal growth and annealing.[10),30)] In pure LGS crystals, the crystal grown in inert gas exhibited higher resistivity than that grown in an oxygen atmosphere.[1)] Then, it is supposed that p-type electric conductivity is dominant in the LGS-type crystal. The carrier is the electric hole in p-type electric conductivity. The holes are generated because of metal vacancy and/or interstitial oxygen in the crystal. This assumption is based on the difference between measured mass density D_m and calculated D_x with $D_m < D_x$ (see Tables 1 and 2). Concerning the Al-substituted crystals, aluminum is substituted for equivalent gallium; hence, this substitution dose not contribute to the decrement of metal vacancy. Compared to pure LTG crystals, LTGA0.5 exhibited higher resistivity in the high temperature range because of the small amount of aluminum ions incorporated into the crystals instead of the gallium ions, which occupy all Ga sites except for the La site, resulting in the decreasing of Ga–O and increasing of La–O distances. Therefore, it can be believed that the Al-substitution inhibits the introduction of interstitial oxygen, resulting in higher resistivity of LTGA0.5 crystals compared with pure crystals.

4. Conclusion

We investigated the structural and piezoelectric properties of the LTGA solid-solution single crystals. The results of single-crystal X-ray structure analysis indicated that Al atoms occupied both octahedral and two tetrahedral sites, maintaining the magnitude of the site preference. The Al substitution of LGS increased d_{14}, whereas it did not affect d_{11}. Through the Al-

substitution, the LTG crystals acquired a higher temperature stability of piezoelectric properties and a higher electric resistivity. The aluminum substituted LTG crystal is a promising candidate for high performance applications at high temperatures.

Acknowledgment The authors would like to thank to Prof. T. Shiosaki, Ph.D. T. Nishida and Mr. S. Tanaka of the Nara Institute of Science and Technology for their helps in crystal growth and fruitful discussions about electrical measurements. A part of this study was financially supported by Takahashi Industrial and Economic Research Foundation.

References

1) Y. Ooishi, H. Noma, K. Kishi, N. Ueno, M. Akiyama and T. Kamohara, *J. Ceram. Soc. Japan*, **113**, 700–702 (2005) [in Japanese].
2) P. Krempl, G. Schleinzer and W. Wallnöfer, *Sens. Actuators, A*, **61**, 361–363 (1997).
3) H. Fritze and H. L. Tuller, *Appl. Phys. Lett.*, **78**, 976–977 (2001).
4) H. Takeda, H. Sako, H. Simizu, K. Kodama, M. Nishida, H. Nakao, T. Nishida, S. Okamura, T. Shikida and T. Shiosaki, *Jpn. J. Appl. Phys.*, **42**, 6081–6085 (2003).
5) S. Zhang, Y. Fei, E. Frantz, D. W. Snyder, B. H. T. Chai and T. R. Shrout, *IEEE Trans. Ultrason. Ferroelectr. Freq. Control*, **55**, 2703–2708 (2008).
6) O. A. Buzanov, A. V. Naumov, V. V. Nechaev and S. N. Knyazev, Proc. 1996 IEEE Inter. Freq. Contr. Symp. (1996) pp. 131–136.
7) K. Shimamura, H. Takeda, T. Kohno and T. Fukuda, *J. Cryst. Growth*, **163**, 388–392 (1996).
8) S. Uda, S. Q. Wang, N. Konishi, H. Inaba and J. Harada, *J. Cryst. Growth*, **237–239**, 707–713 (2002).
9) T. Taishi, K. Kato, T. Hayashi, K. Fujiwara, N. Banba, K. Hoshikawa and T. Fukami, *Tech. Rep. IEICE OME*, **105**, 7–10 (2005) [in Japanese].
10) H. Takeda, S. Tanaka, S. Izukawa, H. Shimizu, T. Nishida and T. Shiosaki, Proc. 2005 IEEE Ultrasonics Symp. (2005) pp. 560–563.
11) H. Takeda, S. Tanaka, H. Shimizu, T. Nishida and T. Shiosaki, *Key Eng. Mater.*, **320**, 239–242 (2006).
12) I. H. Jung, T. Fukuda and K. H. Auh, *J. Electroceram.*, **13**, 471–478 (2004).
13) S. Zhang, A. Yoshikawa, K. Kamada, E. Frantz, R. Xia, D. W. Snyder, T. Fukuda and T. R. Shrout, *Solid State Commun.*, **148**, 213–216 (2008).
14) H. Takeda, S. Tanaka, T. Nishida, K. Uchiyama and T. Shiosaki, *Trans. Mater. Res. Soc. Jpn.*, **31**, 11–14 (2006).
15) SAINT and SADABS, Programs for data collection and absorption correction, Bruker AXS Inc., Madison, WI, USA (2000).
16) G. M. Scheldrick, computer code *SHELXL*93, Georg-August-University Göttingen, Germany (1993).
17) IEEE Standard on Piezoelectricity 176-1987 (1987).
18) W. P. Mason, "Piezoelectric crystals, their application to ultrasonics," D. Van. Nostrand, New York (1950).
19) T. Ikeda, "Fundamentals of Piezoelectricity," Oxford Science, Oxford (1990).
20) M. Kumatoriya, H. Sato, J. Nakanishi, T. Fujii, M. Kadota and Y. Sakabe, *J. Cryst. Growth*, **229**, 289–293 (2001).
21) B. V. Mill, A. V. Batushin, G. G. Hodzhabagjan, E. L. Belokoneva and N. V. Belov, *Dokl. Akad. Nauk SSSR*, **264**, 1385–1389 (1982).
22) H. Takeda, K. Sugiyama, K. Inaba, K. Shimamura and T. Fukuda, *Jpn. J. Appl. Phys.*, **36**, L919–L921 (1997).
23) R. D. Shannon, *Acta Crystallogr., Sect. A: Cryst. Phys., Diffr., Theor. Gen. Crystallogr.*, **32**, 751–767 (1976).
24) H. Takeda, M. Kumatoriya and T. Shiosaki, *Appl. Phys. Lett.*, **79**, 4201–4203 (2001).
25) M. Marezio, J. P. Remeika and P. D. Dernier, *Acta Crystallogr., Sect. B: Struct. Crystallogr. Cryst. Chem.*, **24**, 1670–1674 (1968).
26) H. Kimura, T. Numazawa, M. Sato and H. Maeda, *Jpn. J. Appl. Phys.*, **28**, 1644–1647 (1989).
27) J. Bohm, E. Chilla, C. Flannery, H.-J. Fröhlich, T. Hauke, R. B. Heimann, M. Hengst and U. Straube, *J. Cryst. Growth*, **216**, 293–298 (2000).
28) N. Onozato, M. Adachi and T. Karaki, *Jpn. J. Appl. Phys.*, **39**, 3028–3031 (2000).
29) J. Sato, H. Takeda, H. Morikoshi, K. Shimamura, P. Rudolph and T. Fukuda, *J. Cryst. Growth*, **191**, 746–753 (1998).
30) H. Fritze, H. L. Tuller, G. Borchardt and T. Fukuda, *Mater. Res. Soc. Symp. Proc.*, **604**, 65–70 (2000).